

Simulation of dynamic recrystallization for an Al-Zn-Mg-Cu alloy using cellular automaton

Jie Zhang, Zhihui Li*, Kai Wen, Shuhui Huang, Xiwu Li, Hongwei Yan, Lizhen Yan, Hongwei Liu, Yongan Zhang, Baiqing Xiong

State Key Laboratory of Nonferrous Metals and Processes, General Research Institute for Nonferrous Metals, Beijing, 100088, China

ARTICLE INFO

Keywords:

Cellular automaton
Al-Zn-Mg-Cu alloy
Microstructure evolution
Hot deformation

ABSTRACT

A cellular automata (CA) model has been developed to predict and control the microstructure evolution during hot deformation on 7085 aluminum alloy. The initial microstructure and thermal-mechanical parameters were used as the input data of the CA model. To link microstructure evolution with macroscopic flow stress, dislocation density was set as an important internal state variable. The hot deformation behavior of 7085 aluminum alloy was studied by isothermal compression tests under a deformation temperature range of 623–723 K and a strain rate range of $0.001\text{-}1\text{s}^{-1}$ up to true strains of 0.53–1.20. Electron backscattered diffraction technique and the CA model were utilized to systematically investigate the effects of strain, strain rate and deformation temperature on the microstructure evolution, and further to predict the average grain diameter and the recrystallization fraction after deformation. The simulated results were validated by the experimental data to demonstrate the feasibility and predictability of the CA model.

1. Introduction

Al-Zn-Mg-Cu alloys with high strength and fracture toughness have been widely used as the structure materials in aerospace industry [1]. To achieve specify mechanical properties of these aluminum alloys, the hot deformation is commonly selected to process. During hot deformation, aluminum alloy undergoes different cycles of heating, holding, deformation and cooling, which leads to the occurrence of static recrystallization (SRX), meta-dynamic recrystallization (MDRX) and dynamic recrystallization (DRX) [2]. These processes significantly change the microstructure of materials and then affect the mechanical properties of final products. In order to meet the strict new requirements from the aeronautic industry, it is necessary to control the final microstructure of materials, particularly the grain size [3].

Dynamic recrystallization behavior of Al-Zn-Mg-Cu alloys has been extensively studied. Han et al. [4] found that the increase of recrystallization fraction led to low strength and fracture toughness of 7050 aluminum alloy. Kannan and Raja [5] reported that it was possible to enhance stress corrosion resistance of Al-Zn-Mg-Cu-Zr alloys through inhibiting recrystallization. Therefore, recrystallization has great influence on the mechanical properties of Al-Zn-Mg-Cu alloys [6]. Only grain growth anomaly after recrystallization may degrade the strength, corrosion resistance and toughness of the alloys. After

deformation under optimum temperature and strain conditions, aluminum alloy parts can obtain finer recrystallized grains than that of their casting billets.

The prediction and control of the microstructure is one of the most important issues in the modern aluminum industry [7]. In the rapid development of computer technology and mathematical modeling, it is possible to conduct mesoscale microstructure modeling i.e., on the length scale of the microstructure features using various mesoscopic models, such as cellular automata (CA) method [8–13], Monte Carlo method [14] and Phase Field method [15], etc. These mesoscopic models have the potential not only to provide the average grain size, the volume fraction of recrystallization and stress-strain curve, but also to describe the actual microstructure evolution, such as the morphology and distribution of grain structures. Since a novel algorithm describes the discrete spatial and temporal evolution of microstructure in a mesoscale, CA has been applied to successfully simulate some individual phenomena, such as dynamic recrystallization, static recrystallization and phase transformation [16].

In this work, the hot compressed deformation experiments were carried out to investigate the recrystallization behavior of 7085 aluminum alloy. A CA model was developed to predict the microstructure evolution during hot compression. The developed CA model was verified by the experimental data. A good agreement was found between

* Corresponding author.

E-mail address: lzh@grinm.com (Z. Li).

the simulated and experimental results.

2. Model description and experimental details

Cellular automata are one type of algorithms to describe the discrete spatial and temporal evolution of complex systems based on local deterministic or probabilistic transformation rules to the cells of a lattice [17]. These rules determine the state of a cell as a function of the state of the cell itself and the state of the neighboring sites. The dynamic evolution of the automata can be obtained through the application of these rules. In order to simulate the DRX behavior of 7085 aluminum alloy, the simulation space is first discretized by an array of equally shaped quadratic cells of 912×912 sites, which consist of a regular lattice of cells. The whole lattice corresponds to a real domain of $912 \times 912 \mu\text{m}$. In the present work, each cell has three state variables: (1) a dislocation density variable that describes the deformation-stored energy; (2) a grain label variable that represents different grains; (3) a recrystallization number variable that denotes the number of recrystallization.

2.1. Model of dislocation density evolution

A large number of dislocations appear in the alloys during hot deformation. Generally, the dislocations are created due to work hardening and annealing during dynamic recovery and dynamic recrystallization. To explain the deformation behavior of 7085 aluminum alloy, the Kocks-Mecking model has been employed [18–21]:

$$\frac{d\rho_{i,j}}{d\varepsilon} = K_1 \sqrt{\rho_{i,j}} - K_2 \rho_{i,j} \quad (1)$$

where K_1 is the parameter representing working hardening; K_2 is the parameter representing dynamic recovery and dynamic recrystallization; $\rho_{i,j}$ is the dislocation density of site (i, j) ; ε is the true strain. It is assumed that the initial dislocation density is ρ_0 when $\varepsilon = 0$, applying the boundary condition, (Eq. (1)) can be expressed as:

$$\rho_{i,j} = \left(\frac{K_1}{K_2} - \frac{K_1}{K_2} e^{-\frac{K_2}{2}\varepsilon} + \sqrt{\rho_0} e^{-\frac{K_2}{2}\varepsilon} \right)^2 \quad (2)$$

The relationship between the flow stress and the dislocation density can be described as:

$$\bar{\rho} = \frac{1}{N_c} \sum_{i,j} \rho_{i,j} \quad (3)$$

$$\sigma = \alpha \mu b \sqrt{\bar{\rho}} \quad (4)$$

where N_c is the total number of the cells; μ is the shear modulus; b is the Burger's vector; $\bar{\rho}$ is the mean dislocation density; the correlation constant between stress and dislocation density α is set as 0.5 in the present simulation.

2.2. Model of nucleation

Modeling of the nucleation process is based on experimental observations during incipient recrystallization. The observed nucleation occurs dominantly along grain boundaries and triple junctions of the deformed grains, where DRX will occur once the dislocation density increases to the critical value.

The critical dislocation density ρ_c can be calculated from the following equation [22,23]:

$$\rho_c = \left(\frac{80\gamma_k \dot{\varepsilon}}{3lM_k \mu^2 b^5} \right)^{1/3} \quad (5)$$

where γ_k is the grain boundary energy; M_k is the grain boundary mobility; l is the mean free path of dislocations; μ is the shear modulus. The mean free path of dislocations is calculated as:

$$l = \frac{k\mu b}{\sigma} \quad (6)$$

where k is a constant which is about 10 for most metals.

Starting from the deformed state described by dislocation distributions, the microstructure evolution during hot compression deformation was simulated using probabilistic CA method. The nucleation was assumed to take place in a continuous and probabilistic mode. The normalized parameter $P_{i,j}$ at each site can be calculated from the following equation:

$$P_{i,j} = \frac{1}{2} \frac{\rho_{i,j} - \rho_{min}}{\rho_{max} - \rho_{min}} \mu b^2 \quad (7)$$

where $\rho_{i,j}$ is the dislocation density at the site (i, j) ; ρ_{max} and ρ_{min} are the maximum and minimum dislocation density, respectively. Among the sites, the dislocation density was higher when the normalized parameter was higher than a randomly generated number between 0 and 1.

Here, we consider that the nucleation of DRX only occurs along grain boundaries (including the primary grain boundaries and recrystallized grain boundaries). In the cells that satisfied the nucleation criterion, the state of the cell was switched to be recrystallized and concurrently the dislocation density to zero. The rate of nucleation is given by Ref. [24]:

$$\dot{N} = \frac{1}{4} C_0 \mu^2 b^2 (\rho_{i,j} - \rho_c) \exp\left(-\frac{Q_{act}}{RT}\right) \quad (8)$$

where C_0 is constant; Q_{act} is the activation energy for nucleation; R is the universal gas constant; and T is the deformation temperature.

2.3. Model of growth

The new grains grow at the expense of strain-hardened initial grains. In this process, the dislocation density lowered than before. The migration rate of grain boundary v can be calculated from the following equation:

$$v = mp \quad (9)$$

where m is the grain boundary mobility; and p is the driving force. The grain boundary mobility is a function of T and the disorientation $\Delta\theta$ between each grain boundary site and its neighboring cells as follows [25]:

$$m = m_0 \left(-\frac{Q_b}{kT} \right) \left\{ 1 - \exp \left[5 \left(\frac{\Delta\theta}{15} \right)^4 \right] \right\} \quad (10)$$

where m_0 is the constant for high angle boundary; Q_b is the activation energy for grain boundary movement; k is the Boltzmanns constant.

The driving force p can be expressed as

$$p = \frac{1}{2} \mu b^2 \Delta\rho - \frac{2\gamma}{r} \quad (11)$$

where r is the radius of dynamically recrystallized grain; τ is the dislocation line energy; $\Delta\rho$ is the difference of dislocation density between the growing grains and their neighboring grains; γ is the grain boundary energy. During the simulation, the radius of dynamically recrystallized grain can be calculated from the following equation [26]:

$$r = \sqrt{\frac{N_0 S}{\pi}} \quad (12)$$

where N_0 is the number of cells occupied by the grain; S is the area of a cell.

3. Experimental

The process parameters of hot deformation for aluminum alloys are: The temperature of 623–723 K, the strain rate of $0.001\text{--}1 \text{ s}^{-1}$ and the strain range of 0.51–1.2. The material used in this experiment was the

Table 1

Chemical composition of 7085 aluminum alloy used in the present study.

Elements	Zn	Mg	Cu	Zr	Cr	Fe	Mn	Si	Ti	Al
wt.%	7.94	1.48	1.66	0.14	< 0.01	< 0.01	0.012	0.0028	< 0.01	Bal.

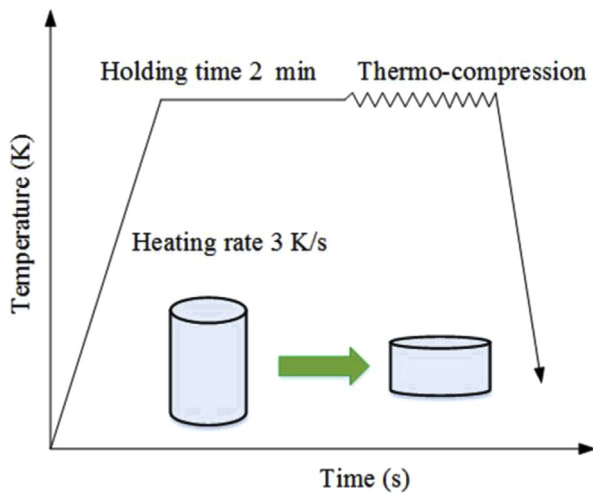


Fig. 1. Workflow of the hot compression test.

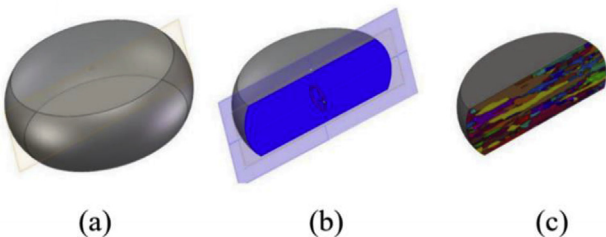


Fig. 2. Schematic representation for cutting plane of compressed samples: (a) deformed specimen; (b) cutting plane; (c) section for EBSD observation.

7085 aluminum alloy ingot with an average grain size of around 224 μm . Its chemical composition is given in Table 1. The ingot was homogenized at 741 K for 36 h and then cooled in room-temperature water. Cylindrical samples with a diameter of 10 mm and a height of 15 mm were machined from the homogenized ingot. The scheme of hot compressive tests is shown in Fig. 1. These tests were carried out in a Gleeble-3500 thermo-mechanical machine. The corresponding experimental procedure is following. Before the compression, the specimens were heated to the deformation temperature at a heating rate of 3 K/s, and then held 3 min at the deformation temperature. Subsequently, the specimens were compressed under a given strain rate, and then quenched in water immediately to freeze the as-deformed microstructure. In order to reduce the friction between the specimens and the press indenters, a graphite lubricant was used during the isothermal compression test. In Fig. 2, the deformed specimens were sectioned parallel to the compression axis along the centerline for microstructure characterization. Electron back scattered diffraction (EBSD) technique and optical microscopy (OM) were used to characterize the specimens in order to obtain information of DRX.

4. Results and discussion

Fig. 3 shows the typical true stress-strain curves of 7085 aluminum alloy obtained after hot compressive tests. The true stress-strain curve for DRX behavior can generally be divided into three stages: working-hardening stage, dynamic softening stage and steady-state stage. The

flow stress increases significantly to the peak value caused by work hardening at the initial stage of deformation, and then decreases attributed to the subsequently occurrence of continuous flow softening. The stress presents a steady-state stage when the further increasing true strain, which indicates the synergistic role of working hardening and dynamic softening.

The initial simulated domain is selected at the cross-section center of the slab with a CA lattice of 912×912 , corresponding to a real domain of $912 \times 912 \mu\text{m}$. The key parameters used in the present CA modeling are listed in Table 2.

Simulation of microstructure evolution during hot compression of 7085 aluminum alloy was performed using the actual experimental parameters, and then the simulated results were compared with the experimental results. Fig. 4 compares the simulated microstructures from the CA model and the experimental results. The different colors in Fig. 4(b) display the different type of grain. The simulated initial microstructure is very close to the experimental results in the grain size and morphology.

The initial microstructure of 7085 aluminum alloy is obtained through simulating grain uniform nucleation and equiaxed growth in CA framework. In order to generate the initial structure closer to the experimental results, cells in the simulation process were randomly selected as nucleus sites in the cell space, while each nucleus cell was numbered, and then gradually grew up until the grains contacted each other. As shown in Fig. 5, the initial microstructure with the prescribed average grain size was generated via running the CA model. In the current model, four different initial microstructures were generated.

By referring to the process parameters of hot deformation experiment of aluminum alloy, the process parameters of thermal simulation test are determined. In Fig. 6, the deformation microstructures of 7085 aluminum alloy under different strains are obtained at 733 K and strain rate of 0.001 s^{-1} . When the true strain is 0.51, no recrystallization occurs in the sample, and the original coarse grains are slightly deformed. When increasing the true strain, the coarse equiaxed grains are flattened and elongated. When the true strain reaches the critical value, some subgrains are observed along the original grain boundaries, where a few fine equiaxed grains appear as well. These distorted fine equiaxed grains grow continuously during the subsequent deformation process to form recrystallization structure. With the increase of true strain, the more serious the grain deformation is, the higher the distortion energy is, and the higher the recrystallization fraction is.

In order to prove that the simulation results are reasonable, we validate the simulation results by thermal simulation experiments. Fig. 7 shows the microstructure development during hot deformation: the original grains are deformed and elongated. During this period, the dislocation density increases progressively particularly near to the grain boundaries because of strain incompatibilities between neighboring grains. If the dislocation density increases above the critical value required for DRX, new DRX nuclei will be generated on the elongated boundaries of the original grains, and then begin to grow. Eventually, the deformed structures are replaced by new recrystallized grains.

Fig. 8 shows the EBSD imaging maps of samples deformed to true strain of 1.20 at 723 K with strain rate of 0.001 s^{-1} . A partially recrystallized necklace microstructure is observed in the sample deformed to true strain of 1.20. The small recrystallized grains that delineated by high angle grain boundaries overlap on the old bulging grain boundaries, especially on triple junctions, indicating the initiation of DRX owing to the strain-induced boundaries migration. Meanwhile, some low angle grain boundaries produced due to dislocation generation and

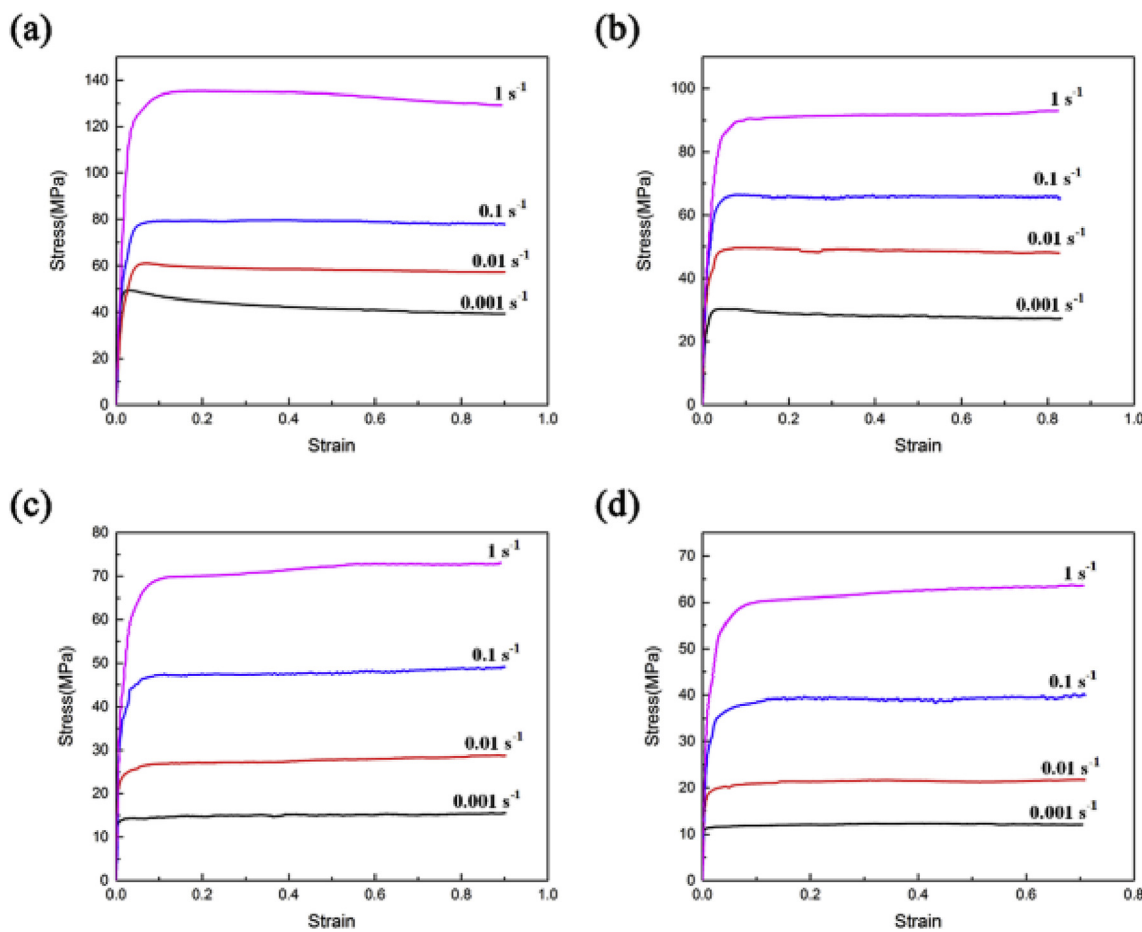


Fig. 3. True stress-strain curves of 7085 aluminum alloy at different temperatures: (a) 623 K; (b) 643 K; (c) 703 K; (d) 723 K.

Table 2
Material constants for 7085 aluminum alloy.

Parameters	Values
Nucleation activation energy Q_{act} (kJ/mol)	313.386
Activation energy for grain boundary movement Q_b (kJ/mol)	117.2
Burger's vector b (m)	2.0×10^{-10}
Shear modulus μ (MN/m ²)	2.69×10^4
Boundary self-diffusion coefficient D_{ob} (m ² /s)	3.8×10^{-4}
Deformation temperature T_m (K)	933.15
Boundary energy γ_m (J/m ²)	0.76

formation of dislocation walls, are detected mainly at the vicinity of original grain boundaries. As seen in Fig. 8 acquired from experiments, the final microstructure was not fully recrystallized in the 723 K and $\dot{\epsilon} = 0.001 \text{ s}^{-1}$. By running the code at 723 K (Fig. 8), similar results are obtained illustrating that the CA model accurately predicted final microstructure.

The deformed microstructure under different true strain was simulated by the CA method, and the simulated results were verified by experimental ones from Gleeb thermal compression test. The fine equiaxed grains along the original grain boundaries were marked with IPP software, and the diameter of each crystal grains was measured to calculate the average grain diameter and recrystallization fraction. The average grain diameter decreases as an increasing in true strain, and the standard error between the simulation results of the average grain

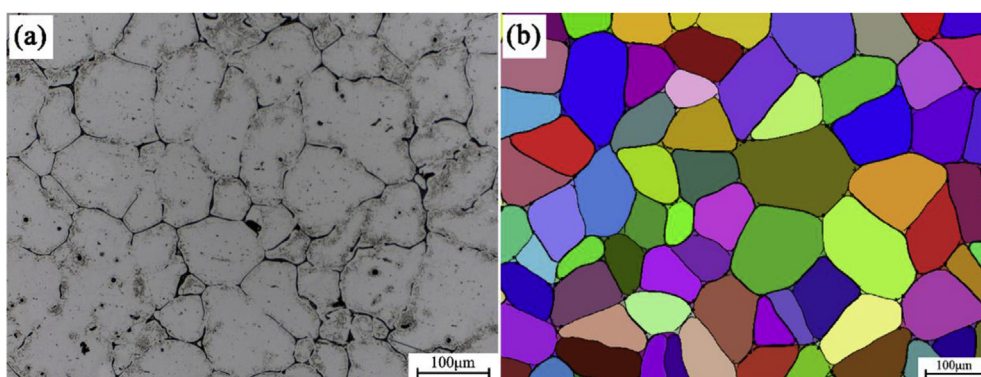


Fig. 4. Comparison of the microstructures of as cast 7085 aluminum alloy obtained by (a) experiment and (b) simulation.

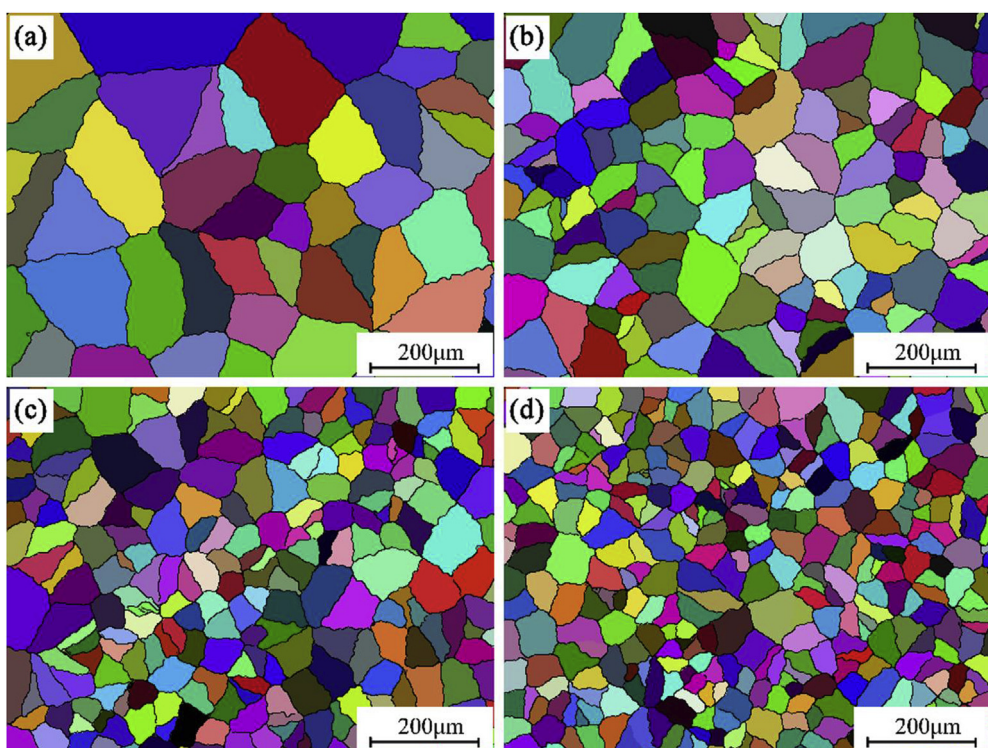


Fig. 5. Initial microstructure with different mean grain radius of: (a) 200 μm , (b) 100 μm , (c) 50 μm , (d) 25 μm .

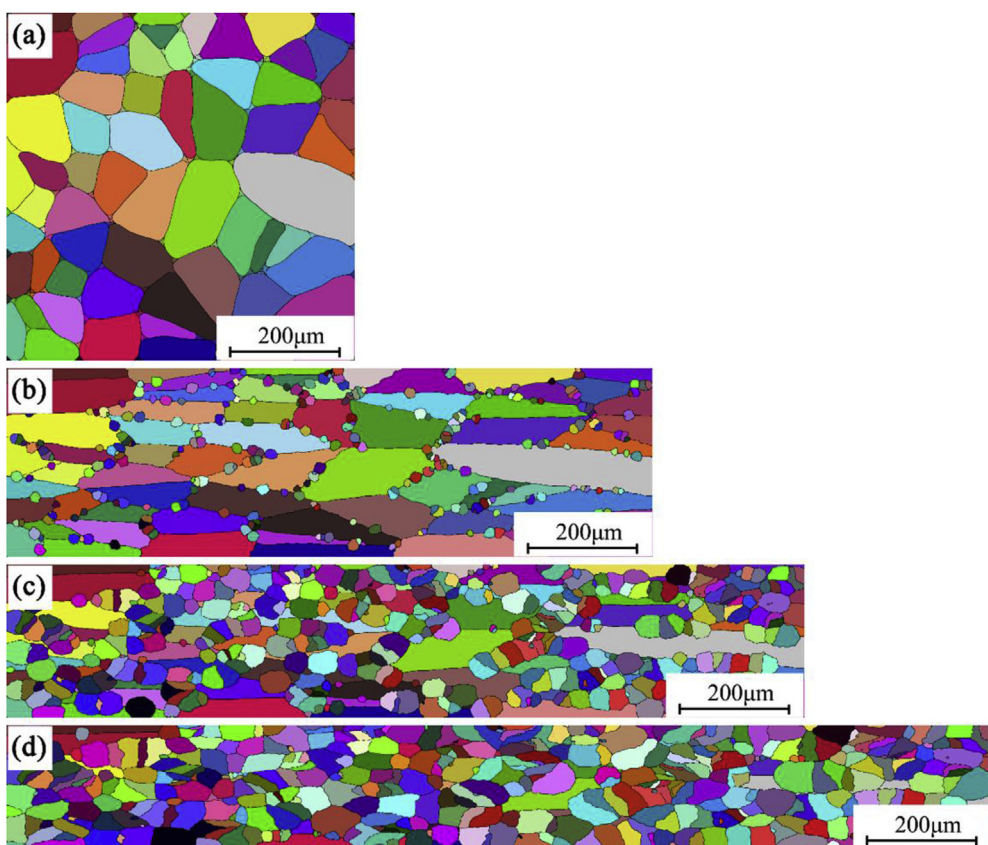


Fig. 6. Simulated microstructure evolution of DRX using CA model at a strain rate of 0.001 s^{-1} and temperature of 733 K. True strains are: (a) $\varepsilon = 0$, initial microstructure, (b) $\varepsilon = 0.91$, (c) $\varepsilon = 1.20$, (d) $\varepsilon = 1.38$.

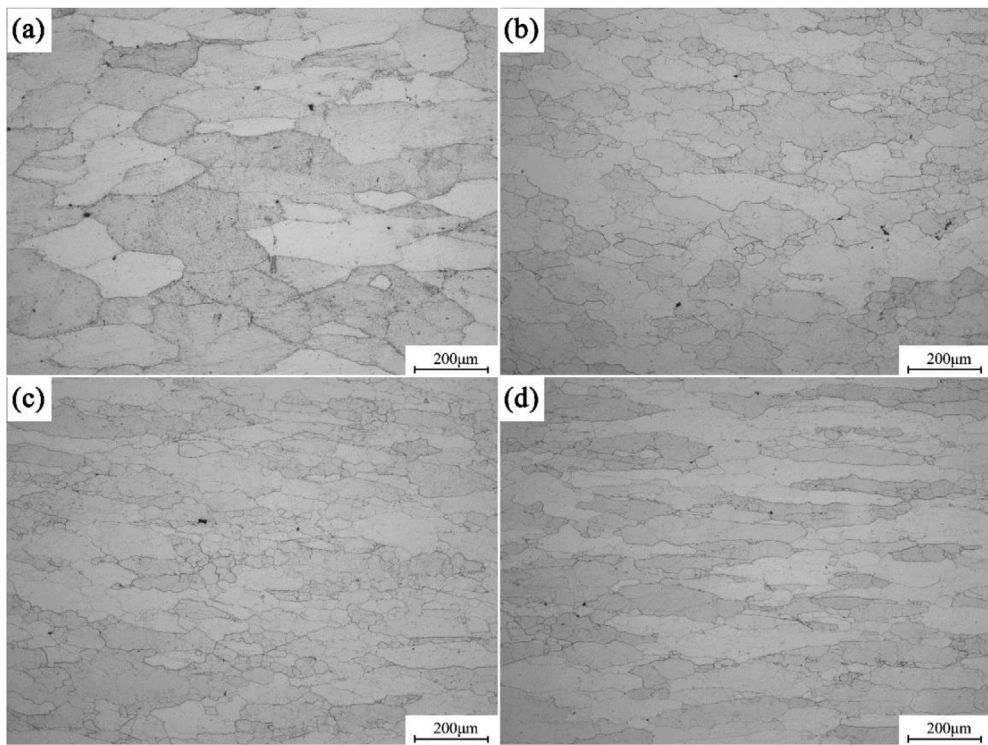


Fig. 7. Typical optical microstructures of 7085 aluminum alloy with (a) $\varepsilon = 0.51$, (b) $\varepsilon = 0.69$, (c) $\varepsilon = 0.91$, (d) $\varepsilon = 1.20$.

diameter and the experimental results are within 15%. Fig. 9 shows the average grain diameter and recrystallization fraction as a function of strain, respectively. The average grain diameter obtained by the simulation is basically consistent with the change trend of experimental ones. When the true strain is less than 0.6, the average grain size of the deformed structure is relatively unchanged, and the recrystallization fraction is 0. When the true strain exceeds 0.6, the average grain diameter rapidly decreases while the recrystallization fraction rapidly

increases.

In Figs. 10 and 11, the experimental results of the average grain diameter and the recrystallization fraction are well consistent with the trend of the simulated results. The average grain size decreases, while the recrystallization fraction increases, as the strain rate decreases. This variation indicates that the reduction of strain rate can promote the occurrence of dynamic recrystallization. At high strain rates, fine equiaxed grains are mainly distributed along the original grain

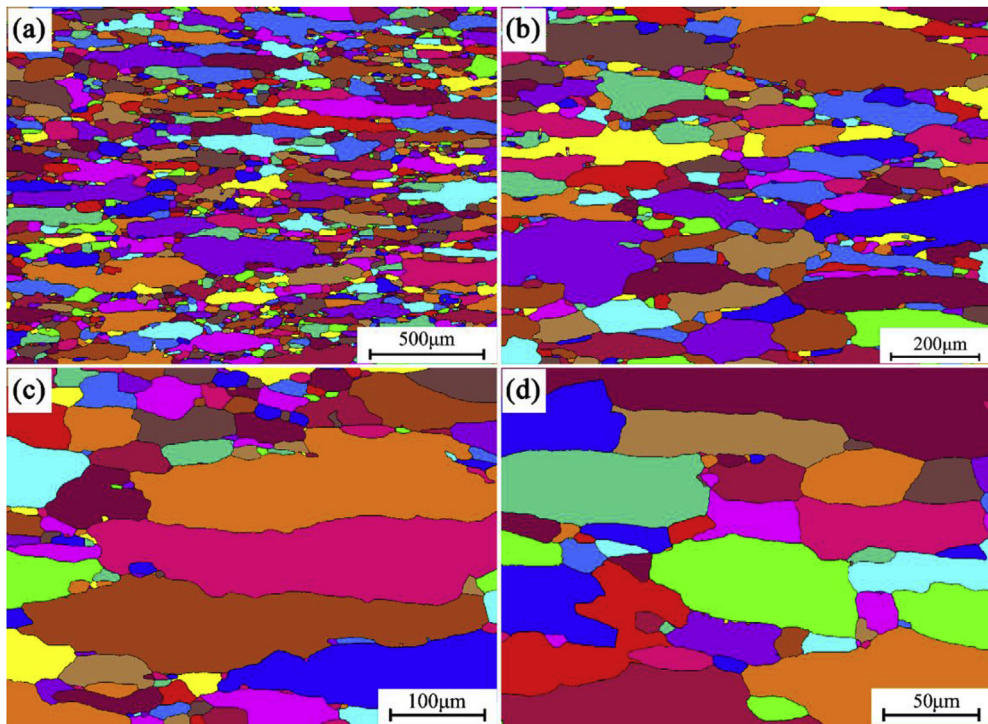


Fig. 8. EBSD imaging maps of samples deformed at true strain of 1.20 at 723 K with strain rate of 0.001 s^{-1} : (a) 50 X, (b) 100 X, (c) 200 X, (d) 400 X.

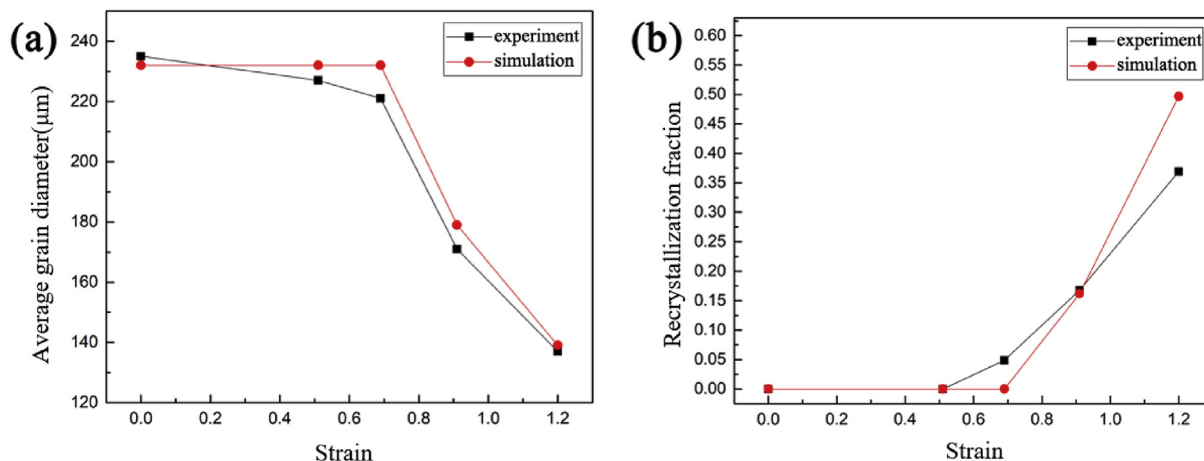


Fig. 9. Average grain size and recrystallization fraction at true strain of 0.001^{-1} and deformation temperature of 733 K: (a) average grain diameter; (b) recrystallization fraction.

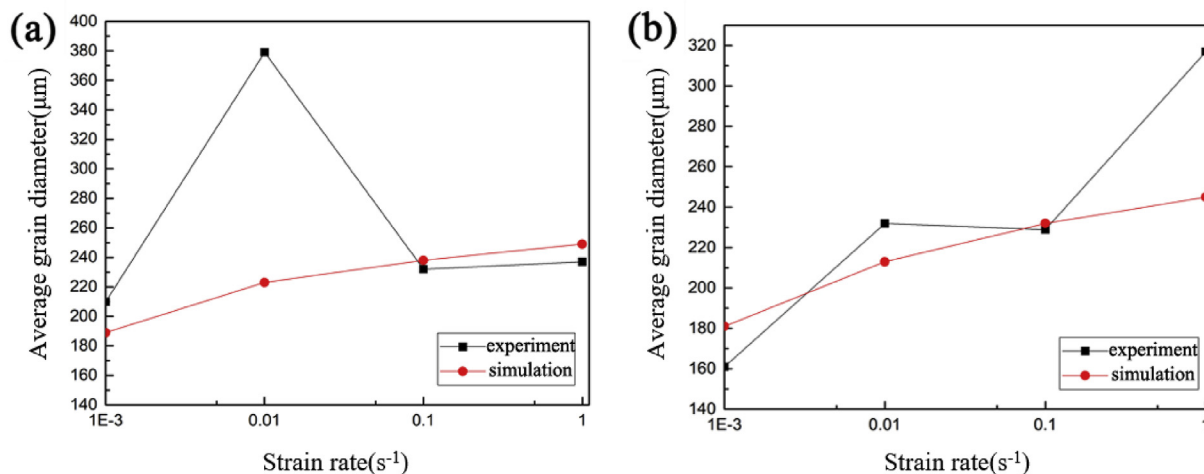


Fig. 10. Average grain diameter at different deformation temperatures ($\epsilon = 0.916$): (a) $T = 703$ K; (b) $T = 723$ K.

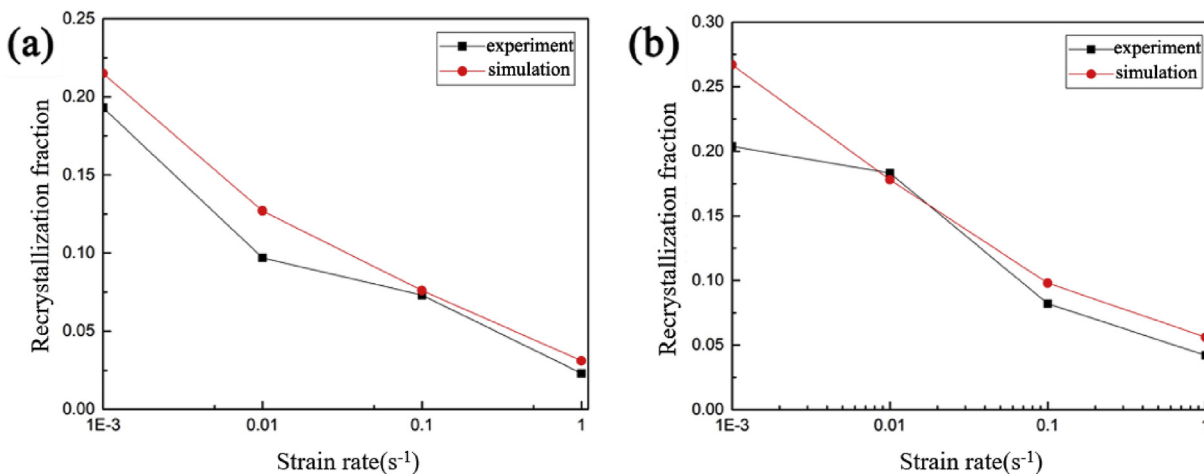


Fig. 11. Recrystallization fraction at different deformation temperatures ($\epsilon = 0.916$): (a) $T = 703$ K; (b) $T = 723$ K.

boundaries and triple junctions. These fine grains are too late to grow due to the short deformation time. At low strain rates, the size of recrystallized grains is large, mainly concentrated along grain boundaries and/or the triangular grain boundaries. The main reason is that the holding time is long at a low strain rate, while the amount of strain increases continuously during the heat preservation process, and

consequently cause the recrystallized grains continue to grow. Dislocations along the grain boundaries, i.e., high distortion energy, can provide more energy for recrystallization nucleation and growth. The internal atoms of the grains tend to be arranged neatly and the distortion energy becomes low. This change is not beneficial to recrystallization nucleation; therefore, there are few crystal grains in the

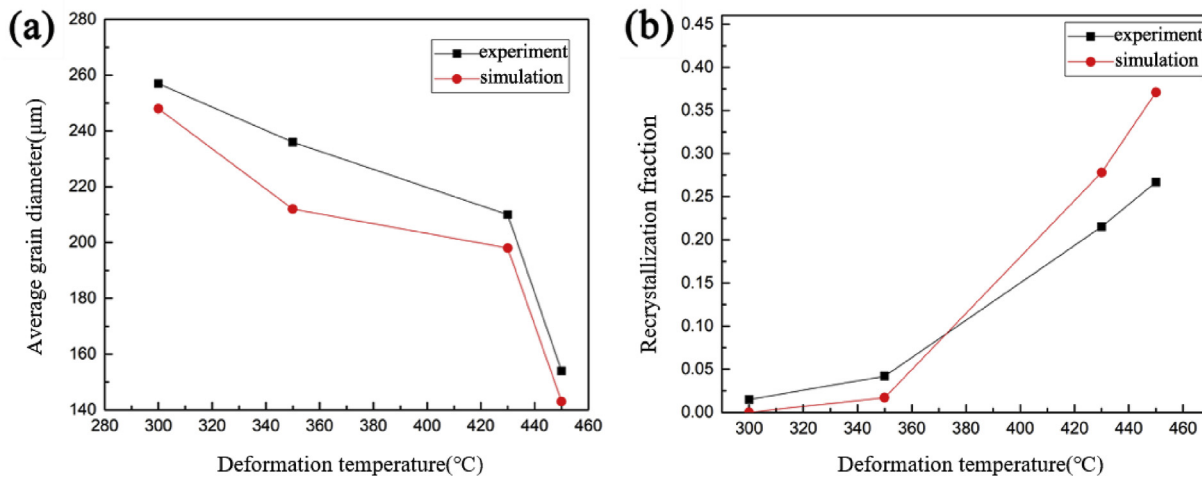


Fig. 12. Average grain diameter and recrystallization fraction at different deformation temperatures.

substrates. The grains nucleation along the grain boundaries gradually engulfs the deformed original grains during the subsequent growth process.

The deformation microstructure at different deforming temperatures was simulated by the cellular automata method, and the simulation results were verified by Gleble thermal compression experiments.

Fig. 12 shows the average grain size and recrystallization fraction curves at different deformation temperatures. The simulation results of the average grain diameter are good consistent with the experimental results. During thermal deformation, the deformation temperature has two effects on the average grain size: one is to provide the necessary energy for nucleation and growth of recrystallized grains, where the recrystallization fraction and recrystallized grain size vary with the deformation; another is to increase the grain boundary mobility and the growth rate of recrystallized grains at elevated temperature, finally to result in coarse recrystallized grains.

5. Conclusions

The microstructure evolution of the 7085 aluminum alloy has been investigated by cellular automaton simulation and experiment. The modified model has been used to predict the average grain diameter and recrystallization fraction under different thermal deformation parameters. The following conclusions can be drawn.

- (1) The simulated results are verified by Gleble thermal compression test. The nucleation rate is determined by the deforming temperature and strain rate. When the true strain is greater than 0.6, obvious recrystallization phenomenon can be observed. At the low strain rate, the recrystallization fraction is higher. It is only possible to trigger recrystallization when the dislocation density exceeds the critical density.
- (2) The recrystallized grains begin to appear along the grain boundaries in the initial microstructure when suffering from a certain plastic deformation, where the dislocation density reaches a critical value. The dislocation density plays an important role in DRX of 7085 aluminum alloy.
- (3) True strain has an important influence on the recrystallization volume percentage and the mean grain size during DRX. Under the same deformation temperature and strain rate, the recrystallization volume percentage increases while the mean grain size decreases as the true strain increases.

- (4) The average grain size of the sample is approximately 224 μm , which is input into the initial generation model to create the initial cell space of the corresponding size. The initial microstructure obtained through the simulation agrees well with the microstructure of the homogenized sample in terms of morphology and grain size in equiaxed grains.

Acknowledgements

This study was financially supported by the National Key and Development Program of China (No. 2016YFB0300803, 2016YFB0300903); National Key Basic Research Development Program of China (2012CB619504).

References

- [1] W. Liu, H. Zhao, D. Li, Z. Zhang, G. Huang, Q. Liu, Mater. Sci. Eng. A 596 (2015) 176–182.
- [2] C.Y. Lin, X.M. Chen, M.S. Chen, Y. Zhou, D.X. Wen, D.G. He, Appl. Phys. A 122 (2016) 1–44.
- [3] M. Zouari, N. Bozzolo, R.E. Loge, Mater. Sci. Eng. A 655 (2016) 408–424.
- [4] N.M. Han, X.M. Zhang, S.D. Liu, D.G. He, R. Zhang, J. Alloys Compd 509 (2011) 4138–4145.
- [5] M.B. Kannan, V.S. Raja, Eng. Fract. Mech. 77 (2010) 249–256.
- [6] D. Li, D.Z. Zhang, S.D. Liu, Z.J. Shan, X.M. Zhang, Q. Wang, Trans. Nonferrous Metal Soc. 26 (2016) 1491–1497.
- [7] D.S. Svyetlichnyy, Comput. Mater. Sci. 60 (2012) 153–162.
- [8] S.I. Kim, Y. Lee, D.L. Lee, Y.C. Yoo, Mater. Sci. Eng. A 355 (2003) 384–393.
- [9] N. Xiao, C. Zheng, D. Li, Y. Li, Comput. Mater. Sci. 41 (2008) 0–374.
- [10] N. Yazdipour, C.H. Davies, P.D. Hodgson, Comput. Mater. Sci. 44 (2008) 566–576.
- [11] G. Kugler, R. Turk, Acta Mater. 52 (2004) 4659–4668.
- [12] R. Ding, Z.X. Guo, Acta Mater. 49 (2001) 3163–3175.
- [13] R.L. Goetz, V. Seetharaman, Scr. Mater. 38 (1998) 405–413.
- [14] B. Radhakrishnan, G. Sarma, T. Zacharia, Scr. Mater. 39 (1998) 1639–1645.
- [15] T. Takaki, Y. Hisakuni, T. Hirouchi, A. Yamanaka, Y. Tomita, Comput. Mater. Sci. 45 (2009) 881–888.
- [16] C. Zheng, N. Xiao, D. Li, Y. Li, Comput. Mater. Sci. 44 (2009) 507–514.
- [17] A. Timoshenkov, P. Warczok, M. Albu, J. Klärner, E. Kozechnik, R. Bureau, Comput. Mater. Sci. 94 (2014) 85–94.
- [18] F. Chen, Z. Cui, J. Liu, W. Chen, S. Chen, Mater. Sci. Eng. A 527 (2010) 5539–5549.
- [19] H.S. Kim, Y. Estrin, E.Y. Gutmanas, C.K. Rhee, Mater. Sci. Eng. A 307 (2001) 67–73.
- [20] U.F. Kocks, H. Mecking, Prog. Mater. Sci. 48 (2003) 171–273.
- [21] H. Hallberg, M. Wallin, M. Ristimaa, Mater. Sci. Eng. A 527 (2010) 1126–1134.
- [22] N. Shen, A. Samanta, H. Ding, Procedia CIRP 58 (2017) 543–548.
- [23] W. Roberts, B. Ahlbom, Acta Metall. 26 (1978) 801–813.
- [24] R. Ding, Z.X. Guo, Acta Mater. 49 (2001) 3163–3175.
- [25] F.J. Humphreys, Acta Mater. 45 (1997) 4231–4240.
- [26] H. Hallberg, M. Wallin, M. Ristimaa, Comput. Mater. Sci. 49 (2010) 25–34.